Chapter 4 *Green Synthesis of HfO_2 Nanoparticles for their Sensing Application*

4.1 Introduction

Now-a-days, green synthesis is gaining popularity over conventional synthesis methods as it is environment-friendly, cost-effective and non-toxic. We have developed a method for the synthesis of HfO_2 nanoparticles using commonly available orange peel extracts and investigated their structure, microstructure and optical properties as described in section 4.2. Subsequently, in section 4.3, we have reported a sensing framework to detect liquid NH_3 with these nanoparticles using electrochemical impedance spectroscopy for its initial performance assessment. We have successfully detected 50 to 500 ppm of liquid NH_3 concentration with charge transfer resistance as the sensing parameter. A prediction model based on charge transfer resistance shows an R^2 value of 0.95 to predict liquid NH_3. In section 4.4, we have summarized the key results of this chapter.

4.2 Green Synthesis and Characterizations

4.2.1 Green Synthesis and Mechanism

To minimize the environmental impact, green synthesis routes have been utilized successfully to synthesize various metal oxide nanoparticles. Nanocomposite ZnO–Ag is synthesized using the leaf extract of *Thymus vulgaris,* which is employed for antimicrobial activity, biocompatibility and solar photocatalysis [54]. Luque *et al.* investigated the influence of different amounts of orange extract on the homogeneity of the size and shape of ZnO nanoparticles [145]. Orange peel extract, a primary byproduct

of the widely available fruit orange, contains several antioxidants. Antioxidants contain aromatic hydroxyl groups, which help in the reduction and stabilization of nanoparticles [145,146]. Hence, orange peel extracts can be used as the reducing and stabilizing agents for synthesizing HfO_2 nanoparticles.

We have successfully synthesized HfO_2 nanoparticles using the orange peel extracts and calcined aliquots of the sample at 600 to 900 °C for different time periods. HfO_2 samples calcined at 900 °C for 1 hour show sharp XRD peaks. Thus, we have fixed the calcination temperature of all HfO_2 samples synthesized using different concentrations of OPE at 900 °C for 1 h. The time for calcination of green synthesized HfO_2 is lesser than the reported calcination time of conventionally synthesized HfO_2 as the organics present in the orange peel extract act as fuel during the calcination, facilitating a combustion-like reaction. The yields of all the samples are greater than 90%. The HfO_2 nanoparticles synthesized using 1 wt% orange peel extract (OPE) is denoted as HO-1-OPE. Similarly, the HfO_2 nanoparticles synthesized using 2 and 4 wt% OPE were denoted as HO-2-OPE and HO-4-OPE, respectively. **Figure 4.1** represents the chemical mechanism of synthesis of HfO_2 nanoparticles utilizing orange peel extracts as reducing and stabilizing agents [55]. This mechanism diagram is drawn using the ChemDraw Ultra 12.0 software. The formation of the HfO_2 nanoparticles by the orange peel extracts is due to the presence of biomolecules (such as flavonoids, limonoids, and carotenoids) [145]. The peel extracts having these biomolecules work as the mediator for ligation. The aromatic hydroxyl groups in the biomolecules develop complexing agents together with the hafnium chloride by the ligation of hafnium ions. After subsequent nucleation and reverse micellization, this triggers the shaping of nanoparticles by reduction and ripening. Subsequently, when calcined at a suitable temperature, HfO_2 nanoparticles are formed by direct decomposition [145,146].

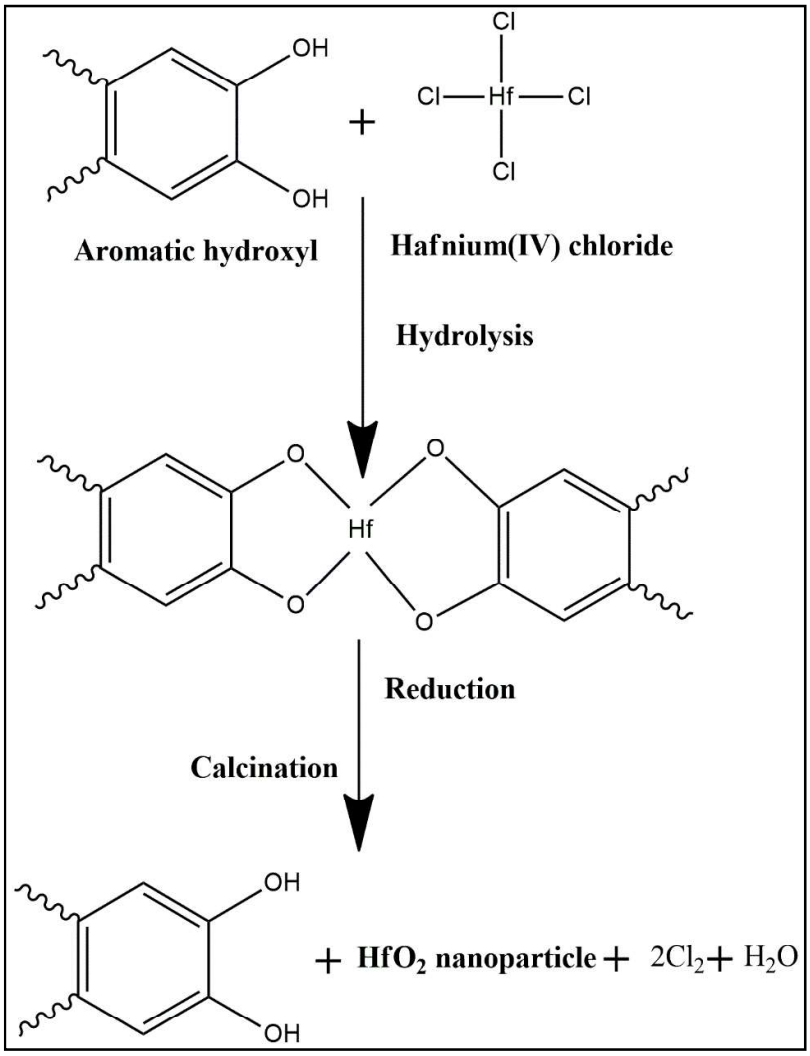

Figure 4.1 *Chemical mechanism of green synthesis of HfO_2 nanoparticles using orange peel extracts.*

4.2.2 Structure, Microstructure and Optical Properties

X-ray diffraction patterns of green synthesized HfO_2 nanoparticles are illustrated in **Figure 4.2**. The sharp diffraction peaks corresponding to (011), (110), (-111), (111), (020), (200), (021), (-211), (112), etc. are indexed according to the monoclinic phase of HfO_2 ($P2_1/c$) with JCPDS number: 78–0049.

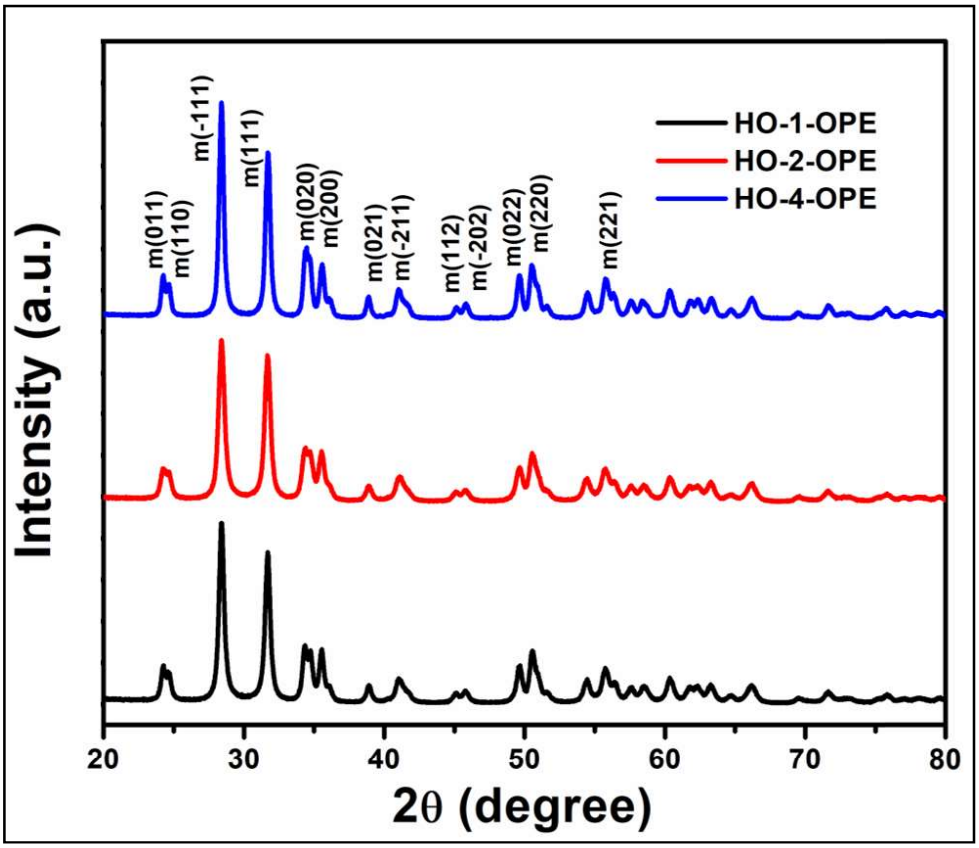

Figure 4.2 *XRD patterns of green synthesized HfO_2 nanoparticles (HO-1-OPE, HO-2-OPE and HO-4-OPE).*

Transmission electron micrographs of the green synthesized HfO_2 nanoparticles are shown in **Figure 4.3**. The micrographs show that HO-1-OPE and HO-2-OPE samples are

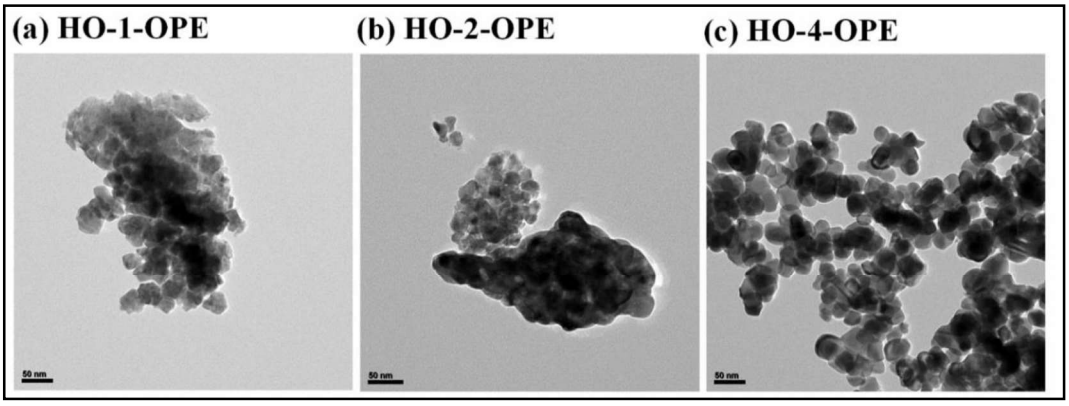

Figure 4.3 *Transmission electron micrographs of (a) HO-1-OPE, (b) HO-2-OPE and (c) HO-4-OPE.*

agglomerated in large clusters (**Figure 4.3 (a)** and **(b)**). The TEM micrograph of HO-4-OPE shows the nanoparticles are well dispersed (**Figure 4.3 (c)**) due to the presence of adequate biomolecules in 4 wt% OPE responsible for the reduction and capping. We have used HO-4-OPE for the sensing layer in electrochemical impedance spectroscopy measurements. A typical Le Bail refinement plot of HO-4-OPE is shown in **Figure 4.4 (a)**. Structural cell parameters of HO-4-OPE obtained by Le Bail refinement with $P2_1/c$ space group are: a = 5.118 Å, b = 5.175 Å, c = 5.29 Å and volume = 138.31 $Å^3$. The refined cell parameters match well with the standard cell parameters of monoclinic HfO_2 nanoparticles [147]. The average crystallite size of the HO-4-OPE is estimated from the Williamson-Hall plot depicted in **Figure 4.4 (b)** [129]. Extracted values of average crystallite size and lattice strain for HO-4-OPE are 34 nm and 0.00182, respectively.

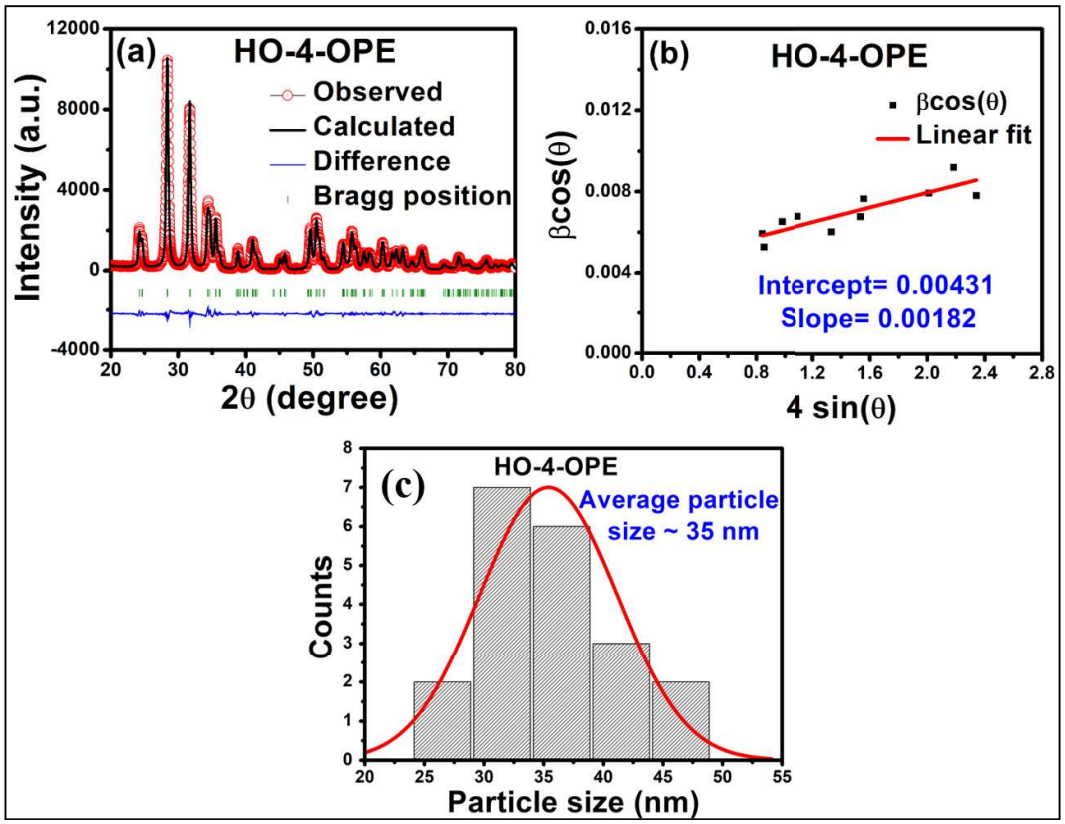

Figure 4.4 *(a) Le Bail profile fitting, (b) Williamson-Hall plot of HfO_2 sample and (c) average particle size histogram of HO-4-OPE.*

The average particle size of the HfO_2 samples is obtained from the transmission electron micrographs, utilizing the ImageJ software by taking the distance between the farthest points of each particle. In **Figure 4.4 (c)**, the histogram shows the average particle size of HO-4-OPE is 35 nm. This value is very close to the average crystallite size obtained from the Williamson-Hall plot for HO-4-OPE, which confirms the dispersive nature of the nanoparticles.

UV-visible absorption spectra of HfO_2 samples synthesized using different concentrations of OPE are depicted in **Figure 4.5**. HO-4-OPE shows the absorption edge and absorption peak corresponding to HfO_2. The peak centered at 215 nm is ascribed to the absorption band of HfO_2 [147]. The absorption spectra of other samples do not show any absorption edge or peak in the 200-800 nm wavelength range. Large, agglomerated

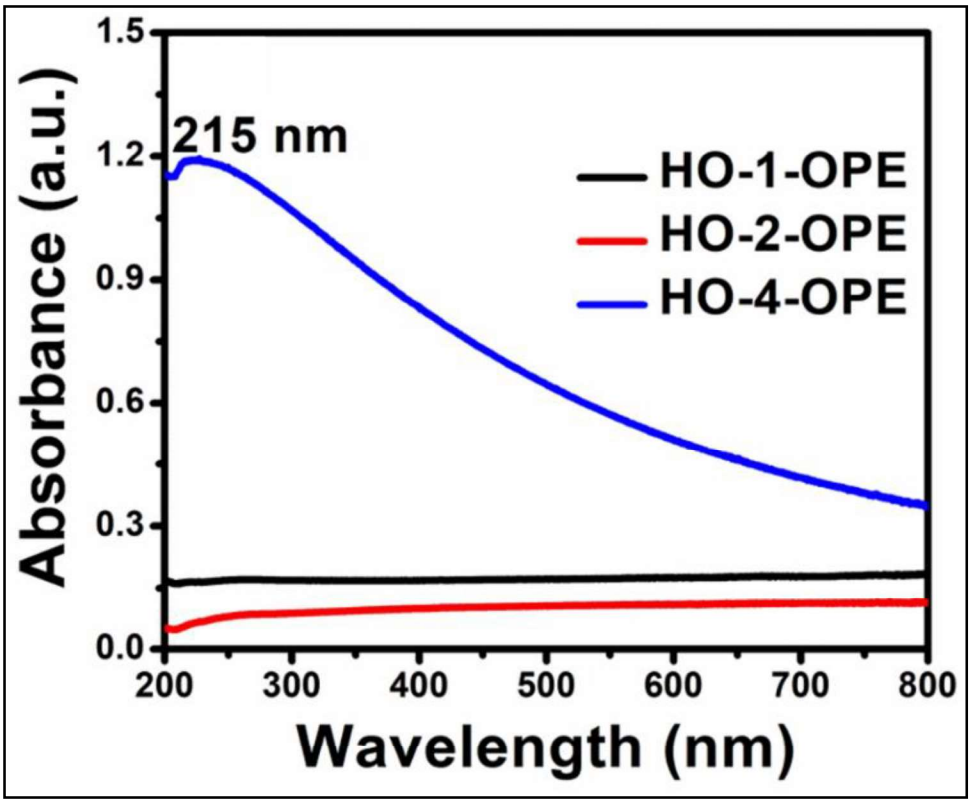

Figure 4.5 *UV-visible absorbance spectra of HO-1-OPE, HO-2-OPE and HO-4-OPE.*

particles do not show absorption peaks due to a decrease in the total surface area. From this information, we can observe that HO-4-OPE is more dispersed than HO-1-OPE and HO-2-OPE. This can also be seen from the TEM images of HfO_2 samples. Hence, we used HO-4-OPE as the active material for the liquid ammonia sensing device fabrication.

4.3 Liquid Ammonia Sensing using Electrochemical Impedance Spectroscopy

Electrochemical impedance spectroscopy (EIS) is a non-destructive technique used for analyzing the interfacial properties and frequency dependent resistance of the electrochemical systems. In EIS, ac signal is applied to the working electrode, and the corresponding response is recorded. The redox species-electrode interactions include the concentration of electroactive species and charge transfer from the electrolyte to the electrode surface in addition to the resistance of the electrolyte. Here, the Bode plots obtained from EIS measurements at different liquid ammonia (NH_3) concentrations are shown in **Figure 4.6**. We can observe the clear changes in the Bode plots with the change in ammonia concentrations. The obtained Bode plots are fitted using the equivalent circuit shown in the inset of **Figure 4.6**, having two constant phase elements (CPEs) in series. The total impedance of the equivalent circuit is:

$$Z(w) = R_s + \frac{1}{Y_0 1(jw)^{\alpha 1} + 1/R1} + \frac{1}{Y_0 2(jw)^{\alpha 2} + 1/R2} \quad \textbf{(4.1)}$$

where, R_s=solution resistance, $Y_0 1$ and $Y_0 2$ are the capacitance of CPE 1 and CPE 2, w is the angular frequency, $\alpha 1$ and $\alpha 2$ values are <1, and $R1$ and $R2$ are the charge transfer resistances. In this work, we have considered the charge transfer resistance ($R1$) through the double layer formed at the interface of the electrode and analyte, as the sensing parameter. Nyquist plots obtained from EIS measurements at different liquid ammonia

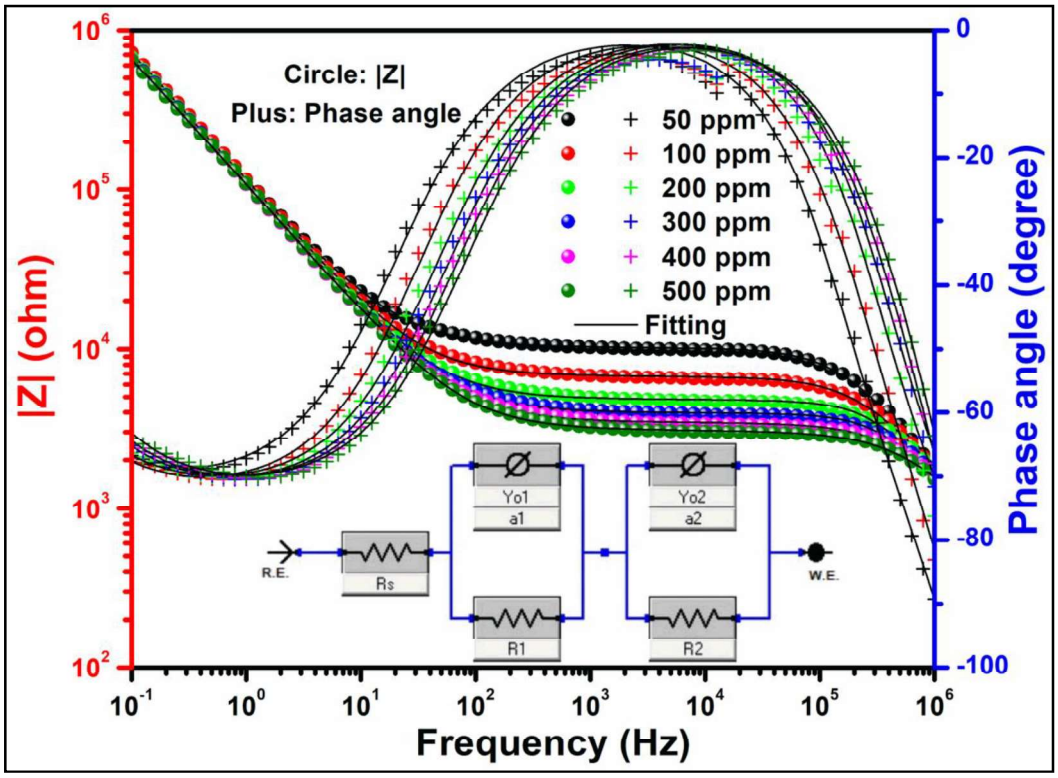

Figure 4.6 *Bode plots obtained from EIS measurements at different liquid ammonia concentrations with 10 mV ac voltage in 100 mHz to 1 MHz frequency range. Inset represents the model used for the fitting.*

concentrations are depicted in **Figure 4.7**. The Nyquist plots are fitted using the same equivalent circuit shown in the inset of **Figure 4.6**. From the Nyquist plot, we can observe the decrease of charge transfer resistance with an increase in the ammonia concentration. For the liquid NH_3 sensor, the electrochemical reaction takes place at the surface of the working electrode. Liquid NH_3 is catalyzed by the superoxides (O_2^-) adsorbed on the surface of the electrode by O_2 vacancies [148]. The nitrification of NH_4^+ into nitrate ions (NO_3^-) occurs in such a process. The chemical equation for the nitrification process is:

$$NH_4^+ + 2O_2^- \rightarrow NO_3^- + H_2O + 2H^+ \quad (4.2)$$

Sufficient energy is released during oxidation, which enables the electrons to jump to the conduction band and hence reduces the resistance of the material [149]. It is known that when phase angle is -90°, the system shows pure capacitive behavior and for -45° phase

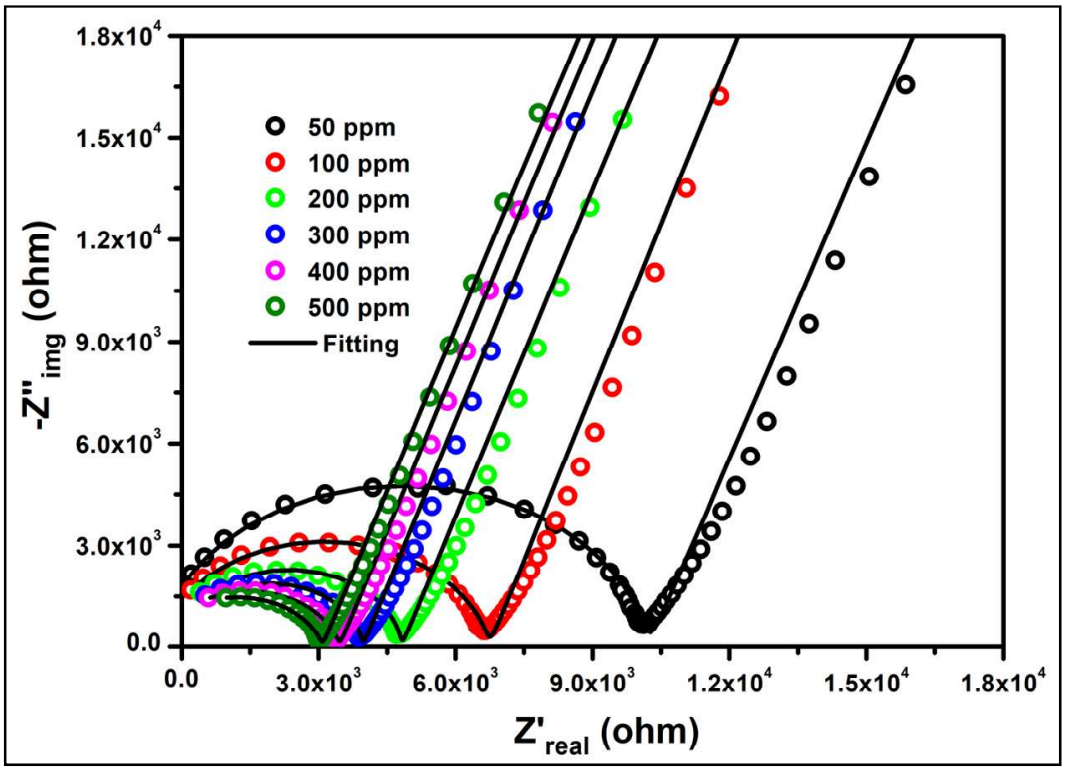

Figure 4.7 *Nyquist plots obtained from EIS measurements at different liquid ammonia concentrations with 10 mV ac voltage in 100 mHz to 1 MHz frequency range.*

angle, it becomes diffusive. Here, we observe from the Bode plot (**Figure 4.6**) that the phase angle changes from ~ -90° to ~ -60° when the concentration of liquid ammonia increases from 50 to 500 ppm, indicating an increase in diffusion. The increase in diffusion causes a decrease in the charge transfer resistance which corroborates with the Nyquist plots. The variation of charge transfer resistance for HfO_2 coated screen printed electrode with respect to ammonia concentrations is modeled using an exponential decay function, as shown in **Figure 4.8 (a)**. The R^2 value for the model is 0.99. We further developed a prediction model to predict ammonia concentration in ppm from the charge transfer resistance. The developed exponential model is represented in **Figure 4.8 (b)** provided an R^2 value of 0.95, demonstrating the high potential of this developed sensing method. This method is selective for liquid NH_3 over ethanol, methanol and acetone.

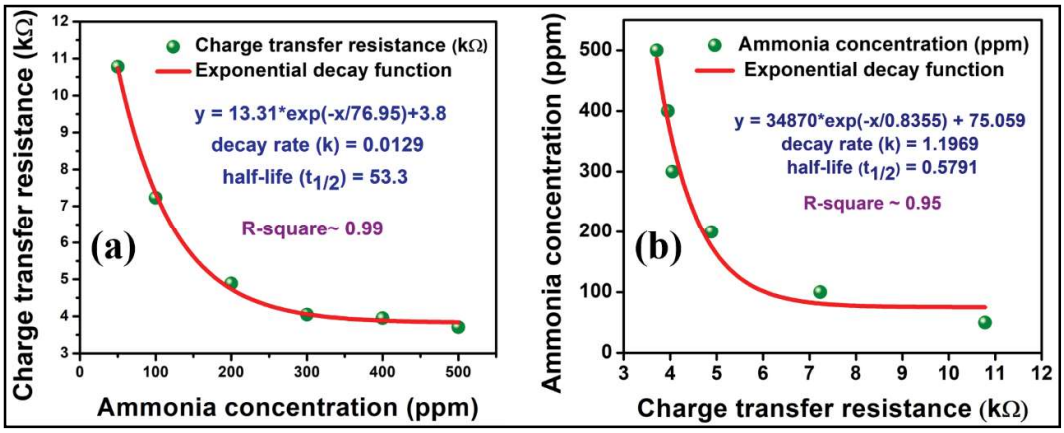

Figure 4.8 *(a) Variation of charge transfer resistance with respect to ammonia concentrations and (b) prediction model to predict ammonia concentration of real samples.*

4.4 Conclusions

We successfully synthesized HfO_2 nanoparticles through the green synthesis technique using orange peel extracts as the biomaterials and characterized them with XRD, TEM, and UV-visible spectroscopy for structural, microstructural, and optical properties. HfO_2 synthesized with 4 wt% orange peel extract and calcined at 900 °C for 1 hour (HO-4-OPE) demonstrated well dispersed crystalline nanoparticles. The average crystallite size of HO-4-OPE was 34 nm which is very close to the average particle size (35 nm) estimated from the TEM micrograph). A sensing framework was further developed for liquid ammonia detection at 6 targeted concentrations in 50-500 ppm range using electrochemical impedance spectroscopy. The charge transfer resistance showed an exponential relationship with concentrations of ammonia with R^2 of 0.99. The prediction model based on the charge transfer resistance showed an R^2 of 0.95 to predict liquid NH_3 concentrations (50-500 ppm). These findings show promises and need to be further validated with a larger number of samples and acquired data sets.